https://doi.org/10.5194/egusphere-2025-241
Preprint. Discussion started: 10 February 2025

Towards sensible heat flux measurements with fast-response fine-wire platinum resistance thermometers on small multicopter uncrewed aerial systems.

Norman Wildmann[1] and Laszlo Györy[1]
[1]Deutsches Zentrum für Luft- und Raumfahrt e.V., Institut für Physik der Atmosphäre, Oberpfaffenhofen, Germany
Correspondence: Norman Wildmann (norman.wildmann@dlr.de)

Abstract. This study demonstrates the feasibility of measuring temperature variance and sensible heat flux with self-calibrated fine-wire platinum resistance thermometers (FWPRT) on multicopter drones. The sensors are especially designed for light-weight, fast response-times and to be carried on miniature drones for turbulence measurements. A significant improvement was found in vertical profiling of temperature gradients compared to slower solid-state sensors, demonstrating reduced hysteresis between ascent and descent phases and accurate representation of strong gradients. More than 100 single flights with the sensors attached to drones of the SWUF-3D fleet were carried out in vicinity to a meteorological mast array at the WiValdi wind energy research park in Northern Germany. The comparison to sonic anemometers shows that mean temperature and temperature variance can be accurately measured within the background flow variability. The same applies for sensible heat flux, which was measured for the first time with multicopter UAS and the eddy covariance method. Sensible heat flux is a crucial parameter to understand the energy balance of the atmospheric boundary layer. An uncertainty below 50 W m^{-2} was determined with the constraint that only low wind speed conditions could be used to allow vertical wind speed measurements with the current algorithm. The results indicate that the temperature sensors are suited for sensible heat flux measurements, but further improvements are necessary with regard to vertical wind speed estimates to decrease the overall uncertainty.

1 Introduction

Small uncrewed aerial systems (UAS) are platforms that have been introduced into everyday life within the last decade due to their low cost, good availability, and ease of use. They serve a large variety of applications, including aerial photography and cinematography, but also for scientific Earth observation. In atmospheric sciences, fixed-wing UAS were initially used to collect in-situ measurements, especially in the atmospheric boundary layer (ABL) (van den Kroonenberg et al., 2008; Wildmann et al., 2015). Data collection methods in that case are based on techniques that were established for crewed research aircraft Lenschow et al. (1986). Flow probes and fast-response sensors were installed for the measurement of thermodynamic variables and the derivation of turbulent fluxes Wildmann et al. (2013, 2015). Fixed-wing UAS remain widely used and are becoming standard tools in scientific ABL campaigns (de Boer et al., 2022; Boventer et al., 2024).

This study focuses on small multicopter UAS, which are the most common UAS type and are usually referred to as 'drones'. These systems are easier to operate due to their vertical take-off and landing capability and advanced control systems. In modern

https://doi.org/10.5194/egusphere-2025-241
Preprint. Discussion started: 10 February 2025

atmospheric measurements, they are most often used to collect vertical profiles of wind, temperature, and humidity (Segales et al., 2020; Lappin et al., 2023). For such profiling tasks, similar sensors as in radiosondes can be deployed and provide good accuracy for temperature and humidity (Hervo et al., 2023). Careful consideration of sensor placement and response time is necessary to optimize data quality (Segales et al., 2022), but high-frequency turbulence data cannot be collected with such sensors. The smallest resolvable turbulence scales for multicopter UAS depend strongly on rotor size, drone weight and the flow disturbance that is induced, but also on sensor noise, e.g. due to vibrations (Kistner et al., 2024). Wetz and Wildmann (2022) and Wildmann and Wetz (2022) show that with the DLR SWUF-3D (Simultaneous Wind measurement with a UAS Fleet in 3D) quadrotors, turbulence eddies can be resolved with a frequency up to 2 Hz. However, this has been shown only for wind, not for temperature or humidity. High-temporal-resolution sampling of not only wind but also temperature is important for a better understanding of thermodynamic processes in the ABL, especially buoyancy-driven flows (Lappin et al., 2022). This is also crucial in complex terrain, where thermally driven flows often occur and drive exchange processes in valleys (Pfister et al., 2024). So far, the eddy-covariance technique to measure sensible heat fluxes has not been tried with multicopter UAS, because no systems are available that can measure both, vertical wind speed and temperature at a sufficiently high temporal resolution. Lee et al. (2017) calculated sensible heat fluxes with multicopter UAS, but based on a conditional sampling technique that uses mean surface temperature and mean measured temperature at flight height.

In this study, we present temperature measurements obtained using a platinum fine-wire resistance thermometer (FWPRT), a technique originally applied with fixed-wing UAS (Wildmann et al., 2013). The study wants to answer the following questions:

1. Can FWPRT be placed on a small multicopter UAS so that the measurements represent atmospheric flow and are not significantly disturbed by rotor-induced flow?
2. What is the temporal resolution of the setup and thus the scale of turbulence eddies that can be measured?
3. Do fast temperature measurements in combination with 3D wind estimates from the UAS allow sensible heat flux measurement?
4. What are the uncertainties that can be achieved?

Section 2 describes the sensor design and integration into the UAS, Sect. 3 describes the experimental setup; Sect. 4 gives a description of the applied methods and Sect. 5 shows results of the sensor validation.

2 Sensor design and setup

The implementation of a compact temperature and humidity sensor on a custom UAS requires a design of a sensor carrier that matches the UAS design. We present here what we call the SWUF-T temperature and humidity module. The concept for the SWUF-T module is to provide a robust commercial and factory-calibrated temperature and humidity sensor along-side a fast and self-calibrated fine-wire platinum resistance thermometer (FWPRT). The commercial sensor is of type HYT.R411 (in previous versions HYT271) by Innovative Sensor Technologies (IST AG). The FWPRT consists of a 13 μm platinum wire of

https://doi.org/10.5194/egusphere-2025-241
Preprint. Discussion started: 10 February 2025

approximately 60 mm length, yielding a resistance $R \approx 50\ \Omega$. It is connected to an Analog Devices MAX38165 resistance-to-digital converter chip in a four-wire sensor connection setup. The MAX38165 produces a constant current through a reference resistor (here: 100 Ω) and the platinum wire. The voltage difference is a measure for the resistance of the wire and can be directly converted to a temperature value based on the known temperature-dependent properties of platinum. The I2C interface of the HYT sensors as well as the SPI interface of the MAX38165 are made available at the GH connector of the SWUF-T board, but can also be routed to an Arduino Nano Every Board that can be attached on top. If the Arduino Nano Every is attached, the GH connector provides a UART interface to the Arduino through which both, HYT and FWPRT measurements are transmitted via MAVLink protocol. The latter is the setup which is used in this study to connect SWUF-T measurements to the Pixhawk 4 Mini autopilot board. Figure 1 shows the principle design (a) and pictures of the board without (b) and with (c) sensor housing. The housing is designed to shield the sensors from incoming radiation, while allowing passive ventilation. Wildmann et al. (2013) showed that already slow airspeeds provide sufficient ventilation for forced convection on the thin wire and thus omit radiation effects.

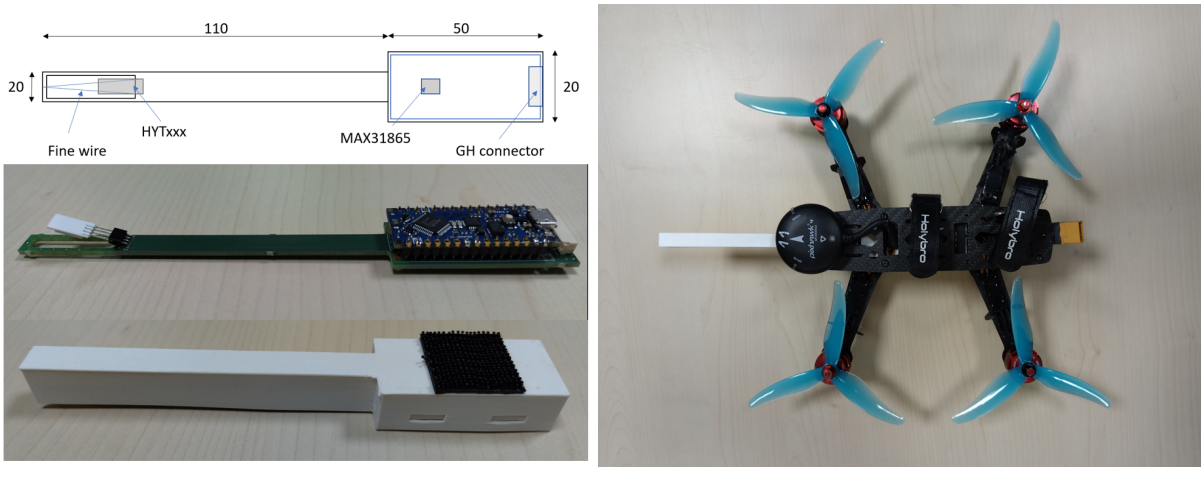

Figure 1. SWUF-T board design concept (a) and pictures of the sensor without (b) and with (c) housing. (d) shows the sensor attached to the QAV250 UAS frame.

Ghirardelli et al. (2023) and Jin et al. (2023) recently showed by means of CFD simulations and field measurements that the best position to place a flow sensor on a multicopter is upstream in front of the rotors. Especially since we are operating with the weather-vane mode that will always point the y-axis of the UAS body-frame into the main wind direction, we place the SWUF-T sensor upstream in the main axis, too. The sensitive elements of the sensor in our setup is 50 mm in front of the rotor plane.

https://doi.org/10.5194/egusphere-2025-241
Preprint. Discussion started: 10 February 2025

3 Experimental setup

3.1 Krummendeich, research wind farm WiValdi

The research wind farm WiValdi at Krummendeich (https://windenergy-researchfarm.com/) in Germany is a facility that is operated by the German Aerospace Center and was instrumented in cooperation with the ForWind universites at Oldenburg, Bremen and Hannover. The meteorological mast array (aka met mast array, MMA), which is a set of two 100 m and one 150 m mast in the center, is a suitable infrastructure to validate spatial measurements in the field with UAS and vice versa (i.e. to determine flow disturbance by the masts). Details about the masts are given in Sect. 4.1.

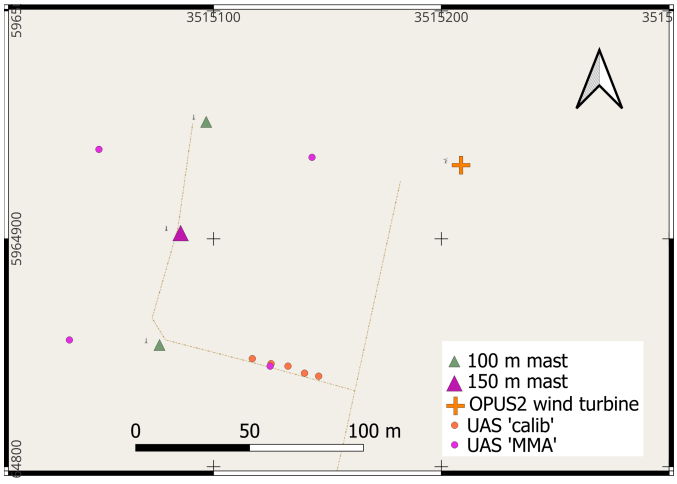

Figure 2. Map of the Krummendeich test site with wind turbine OPUS2 (orange), MMA (triangles) and drone flight positions (red circles). Background map: ©OpenStreetMap contributors 2025. Distributed under the Open Data Commons Open Database License (ODbL) v1.0.

Analyses in this study is based on a campaign that was conducted in July 2024, particularly from 22-25 July 2024, when flights were conducted in close proximity to the mast array. During these days, the wind turbines OPUS1 and OPUS2 at the site were not operating. Figure 2 shows a map with hover positions of the UAS relative to the masts and Tab. 1 gives a list of flights that were used for the analyses with the corresponding meteorological conditions. Two different flight pattern ´MMA‘ and ‘calib´ are listed and correspond to the pink and orange dots of UAS positions in Fig. 2 respectively. The ´MMA‘ pattern was designed to mimic sensor positions of the mast array in a further plane perpendicular to the mast array axis, whereas the ‘calib´ pattern was used to have five UAS as close as possible to each other for cross-calibration of wind and temperature measurements.

3.2 Cochstedt, National Test Centre for Unmanned Aircraft Systems

The National Test Centre for Unmanned Aircraft Systems at the airport of Cochstedt is a facility operated by the German Aerospace Center, specifically designed to support UAS operations with its infrastructure. An airport traffic zone (ATZ) can be

https://doi.org/10.5194/egusphere-2025-241
Preprint. Discussion started: 10 February 2025

Table 1. Measurement flights from 22-25 July 2024

#	t UTC	UAS	pattern	height m	Ψ deg	U m s^{-1}	TI %	T °C
36	22.07.2024 10:10	12,13,24,32,21,15,25	mast array	25, 90	303	8.4	19	16.7
37	22.07.2024 10:50	12,22,13,14,21,15,25	mast array	25, 90	300	8.2	18.4	16.8
38	22.07.2024 11:30	12,22,13,14,24,21,15,25	mast array	25, 90	303	8.0	18.7	16.9
39	22.07.2024 12:30	12,24,32,21,15,25	mast array	25, 90	303	7.9	20.4	17.1
40	22.07.2024 12:55	14,24,21,15,25	mast array	25, 90	300	8.1	20.6	17.2
41	22.07.2024 13:30	12,22,13,14,24,32,21,15,25	mast array	25, 90	292	8.5	18.8	17.3
42	22.07.2024 14:15	12,22,13,14,24,21,15,25	mast array	25, 90	309	7.8	17.4	17.3
43	22.07.2024 14:50	12,22,13,14,24,21,15,25	mast array	25, 90	312	7.5	18.6	17.4
44	22.07.2024 15:15	13,14,24,21,15,25	mast array	25, 90	305	6.6	19.8	17.4
46	23.07.2024 06:40	12,13,15	mast array	25, 90	228	6.6	15.7	19.0
47	23.07.2024 07:20	12,13,14,15	mast array	25, 90	246	5.8	14.5	19.2
48	23.07.2024 07:55	12,14,32,15	mast array	25, 90	256	5.1	21.4	19.4
50	23.07.2024 08:40	12,13,14,32,15	mast array	25, 90	247	6.2	16.5	19.7
51	23.07.2024 09:20	13,14,15	mast array	25, 90	243	5.4	18.4	19.7
52	23.07.2024 09:45	12,13,14,32,15	mast array	25, 90	238	7.1	14.0	19.9
69	25.07.2024 07:45	32,12,13,14,15	calib	99	224	3.9	19.8	15.3
70	25.07.2024 08:15	21,22,23,24,25	calib	99	222	4.0	22.2	15.8
71	25.07.2024 08:50	16,17,18,19,20	calib	99	204	4.6	17.0	16.4
74	25.07.2024 11:55	32,21,23	mast array	25, 90	212	5.0	15.1	19.8
77	25.07.2024 13:00	14,21,24,13,23	mast array	25, 90	204	2.9	27.9	20.5
78	25.07.2024 13:30	32,24,23	mast array	25, 90	214.5	3.6	21.8	21.2

activated up to 3000 feet above ground level to mitigate air risk for UAS operation. We used this possibility to conduct vertical profiles with our SWUF-3D drones in June 2024. Most of the flights were conducted using a newer version and frame of a multicopter; however, we also conducted one flight on June 25, 2024, up to 300 meters in height with the frame as described in Sect. 2 which is used in this study.

4 Methods

4.1 Meteorological mast array

The meteorological mast array (MMA), conceptualized by the University of Oldenburg, features 51 3D sonic anemometers and 32 cup anemometers to measure distributed wind fields within an area covering the rotor diameter of the installed wind turbine at the WiValdi site. The three masts are separated by 50 m, with the central mast reaching 150 m and the outer masts

https://doi.org/10.5194/egusphere-2025-241
Preprint. Discussion started: 10 February 2025

Table 2. List of 3d sonic anemometers at the MMA that were used in this study.

ID	Name	tower	height	boom direction	ΔT_s
500706	MN_B25BS_Z70X4Y1_USA	North	25 m	South	-1 K
500690	MN_ML_Z99X0Y0_USA	North	99 m	Top	0
500772	MS_B25BN_Z70X4Y1_USA	South	25 m	North	-1.2 K
500753	MS_ML_Z99X0Y0_USA	South	99 m	Top	-0.7 K
500727	MC_B100BS_Z70X4Y1_USA	Center	100 m	South	0 K

reaching 100 m. In this study, we use five sonic anemometers as a reference for the drone-based measurements. The position and identification of these sonic anemometers are listed in Table 2.

The sonic anemometers at 25 m height are installed on 7 m booms pointing towards the central mast; those at 99 m are installed on top of the masts to reach their final height. Each Thies Clima 3D sonic anemometer provides three-dimensional wind information in the anemometer's coordinate system and three readings of sonic temperature, which are calculated from the speed of sound and are theoretically equivalent to virtual temperature. Because we lack cross-wind correction parameters according to Liu et al. (2001) for this type of sonic anemometer, we use the median of the three measured temperatures (T_u, T_v and T_w) to obtain a final temperature reading, T_s, as suggested by the manufacturer:

$$T_s = \text{median}(T_u, T_v, T_w) \tag{1}$$

For turbulence and heat flux measurements, accurate absolute temperature is not critical. The raw temperature data from the sonic anemometers is not well calibrated and exhibits offsets compared to the drone measurements and the well-calibrated temperature sensor at the WiValdi site's inflow mast, located approximately 600 m to the west (out of scale in Fig. 2). For the three days of flights analyzed in this study, we apply a rough bias correction based on the inflow mast measurements. Figure 3 shows the uncorrected absolute temperature readings of the two sensors at 99 m (light colors) in the MMA compared to the inflow mast and the bias-corrected values (dark/full colors). The figure shows that the sonic anemometer at the north mast agrees well with the reference, but the south sonic at 99 m has an average bias of -0.7 K. It also shows that the bias correction does not uniformly correct the temperature readings across the full range and for all days. For spatial temperature measurements with the MMA, improved corrections will be necessary in future work if high accuracy is required.

4.2 Virtual temperature

The in-flight performance of the temperature sensor requires validation through field experiments. The preferred method is to fly the UAS in close proximity to sonic anemometers. A sonic anemometer provides a temperature reading derived from the speed of sound, which is equivalent to virtual temperature, T_v. Therefore, all temperature readings from the UAS that are compared with sonic anemometer measurements are converted to virtual temperature. Virtual temperature can be calculated

https://doi.org/10.5194/egusphere-2025-241
Preprint. Discussion started: 10 February 2025

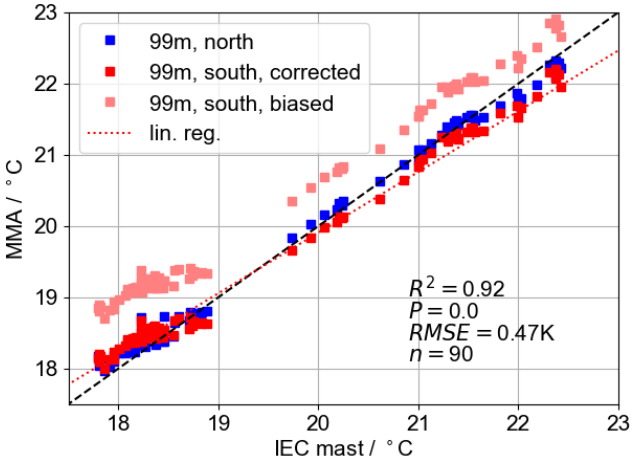

Figure 3. 10-minute mean measurements of temperature of North and South mast sonic anemometer at 99 m compared to a reference temperature sensor at the IEC inflow mast.

from measured temperature, T, barometric pressure, P, and relative humidity, φ, using the saturation water vapor pressure, E, water vapor pressure, e, and mixing ratio, m_h, according to:

$$E = 6.107 \cdot 10^{\frac{7.45T}{235.0+T}} \tag{2}$$

$$e = \varphi E \tag{3}$$

$$r_v = 0.622 \frac{e}{P - e} \tag{4}$$

$$T_v = (T + 273.15)(1.0 + 0.61 m_h) \tag{5}$$

4.3 Sensible heat flux

Using the eddy covariance method, sensible heat flux, H, can be calculated from variations in temperature and vertical wind speed as

$$H = \rho C_p \overline{T_v' w'} \tag{6}$$

where ρ is the air density, C_p is the specific heat capacity of air and $\overline{T_v' w'}$ the covariance of temperature and vertical wind speed. Both variables ρ and C_p can be calculated from thermodynamic measurements made by the drone itself, namely temperature, humidity, and pressure. We apply a correction for moisture to the specific heat capacity of dry air, such that

$$C_p = 1004.67 \text{ J kg}^{-1}\text{K}^{-1} (1 + 0.84 m_h) \tag{7}$$

https://doi.org/10.5194/egusphere-2025-241
Preprint. Discussion started: 10 February 2025

where m_h is the water vapor mixing ratio.

We intentionally calculate sensible heat flux using 10-minute averages, recognizing that a representative sensible heat flux may require longer averaging periods to adequately sample the largest turbulent eddies for the eddy covariance method. However, the purpose of this paper is not to study sensible heat flux itself within the atmospheric boundary layer, but rather to determine the capability of drones equipped with fast temperature sensors to derive sensible heat flux values comparable to those from other in situ sensors, especially in the small scales. At the current stage of development in this study, the SWUF-3D fleet was unable to fly for 30 minutes or longer. The most consistent and comparable dataset was obtained using 10-minute averages.

4.4 Laboratory calibration

The HYT sensors come factory-calibrated with a specified accuracy of 0.2 K in the temperature range $0 \ldots 50\,^{\circ}\mathrm{C}$. The MAX38165 defines a total accuracy of temperature measurements over all operating conditions of 0.5 K. In our setup, we do not use a standard PT100 or PT1000 element, but use a platinum fine wire as specified in Sect. 2. From a known base resistance of the wire at $0\,^{\circ}\mathrm{C}$ (R_0) the actual resistance R_{pt} is a function of temperature T:

$$R_{\mathrm{pt}} = R_0 \left[1 + AT + BT^2\right] \tag{8}$$

The length of the wire varies due to manufacturing inaccuracies, so that $R_0 = 50 \pm 5\ \Omega$ are possible in the manufacturing process. For best accuracy, we calibrate each sensor individually in an EdgeTech RHCal portable calibration chamber with certified and traceable accuracy. Figure 4 shows the calibration curve of five sensors compared to the theoretical curve of a platinum resistance with $R_0 = 50\ \Omega$.

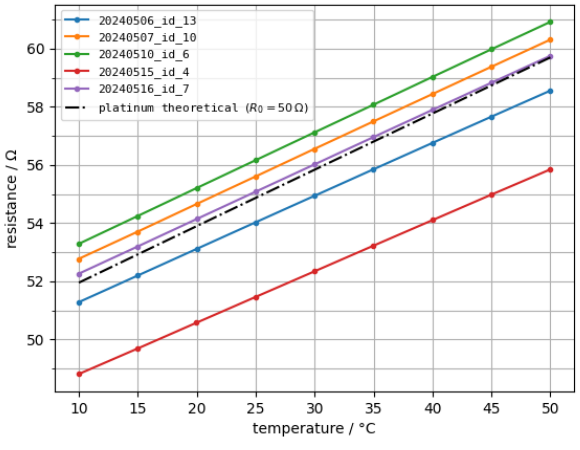

Figure 4. Calibration curve of five individual FWPRT sensors and the theoretical curve of a platinum resistance at $R_0 = 50\ \Omega$ (dashed line).

https://doi.org/10.5194/egusphere-2025-241
Preprint. Discussion started: 10 February 2025

The curves show a strong linear relationship between temperature and resistance, which corresponds to the theoretical expectations. Applying a linear model to the theoretical platinum curve within the considered temperature range results in a coefficient of determination of $R^2 = 1 - 2.86 \times 10^{-6}$, indicating a nearly perfect fit. Similarly, linear models applied to the measurement series produce a median $R^2 = 1 - 6.57 \times 10^{-6}$. These coefficients of determination are well above 0.99 and demonstrate that the sensors can be assigned a linear calibration. Observed deviations are primarily biases, which can be corrected by adjusting resistance values. While an individual bias correction value provides a reasonable approximation, it indicates that the differences in the slopes of the individual curves are too large to achieve the desired precision of less than 0.1 K over the full temperature range. These variations in slope may be attributed to material impurities and production tolerances. Therefore, a slope adjustment is necessary, which can be achieved using a second coefficient, resulting in a first-order calibration equation. Not all 25 temperature sensors, including spares, could readily be calibrated in the calibration chamber so that some were only calibrated with the bias correction. We thus expect an average absolute RMSE$<= 0.5\ K$.

5 Results

5.1 Flow disturbance and sensor placement

From Wetz and Wildmann (2022) and Wildmann and Wetz (2022), we know that the resolution of turbulence with the SWUF-3D fleet is limited to a temporal resolution of approximately 2 Hz, corresponding to a 2.5 m eddy size at a mean wind speed of 5 m s^{-1}. To demonstrate that the flow at these scales is not significantly disturbed at the temperature sensor's position, we visualized the flow using smoke and flew the drone within the plume. At wind speeds of 2–3 m s^{-1}, recorded during the test, it is clear that the flow is significantly disturbed only by the downwash below and downstream of the UAS. Virtually no disturbance is detected directly in front of the UAS. At higher wind speeds, upstream effects will be even smaller. Figure 5 shows a snapshot of the flow visualization. Previous studies using CFD (Ghirardelli et al., 2023) and lidar measurements (Jin et al., 2023) have shown the effects of rotor downwash on sensor position for much larger drones but reached the same conclusion: placement in front of the drone, aligned with the wind direction, is the optimal location. Operating the drone in weather vane mode, i.e., turning the nose into the wind, is essential for good measurement accuracy.

5.2 Average temperature

As typical for such instruments, the sonic anemometers at the met mast array do not provide a precise measurement of the absolute virtual temperature value and were corrected accordingly as described in Sect. 3. To show that the calibrated SWUF-T sensors provide robust temperature readings, we show the comparison of five UAS that were flown in close proximity (calib_pattern, see Sect. 3) in Fig. 6. One of the sensors had electronic problems, so that only four sensors are used for the comparison. In the background, the corrected sonic temperatures at 99 m are shown for the south (solid blue) and center (light blue) mast.

https://doi.org/10.5194/egusphere-2025-241
Preprint. Discussion started: 10 February 2025

Figure 5. Flow visualization with blue smoke.

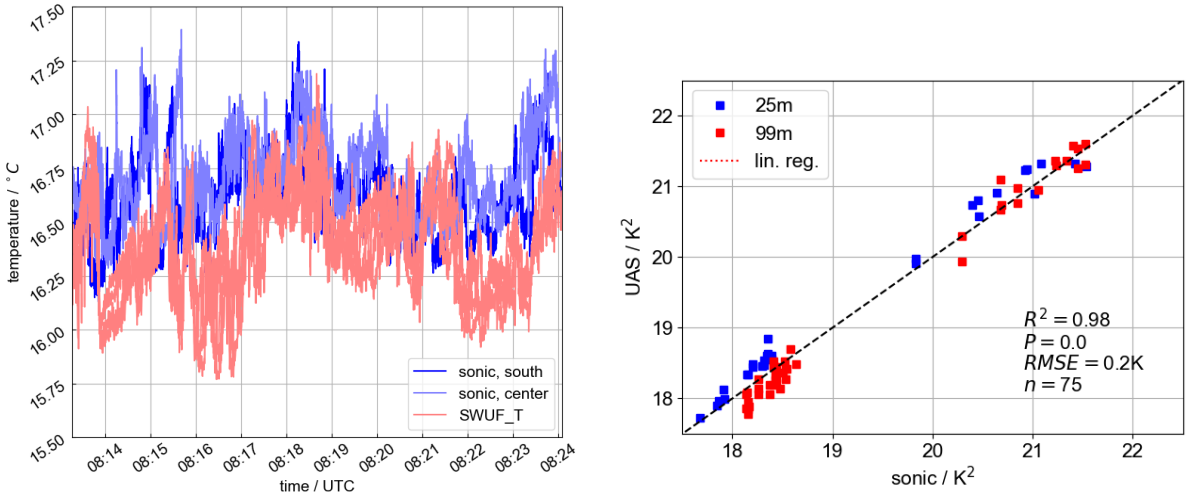

Figure 6. Time series of virtual temperature for four UAS (red) in close proximity to the met mast array and corresponding sonic anemometer readings (blue) for flight #70 (a). Comparison of mean virtual temperature measurements with UAS compared to corrected sonic temperature on closest mast.

The average relative deviations between the four sensors on the UAS are below 0.1 m s^{-1} for this test. The deviations to the sonic anemometers are larger which can be attributed to the distance of 50 m to the mast. It is evident that the fluctuations within the 10-minute period fit better to the south mast anemometer than the center mast which is even further away.

5.3 Vertical profiling

Temperature sensors are known to introduce errors in vertical profiling with UAS (see Cassano (2014) for fixed-wing and Tikhomirov et al. (2021) for multicopters), as well as with radiosondes (Tschudin and Schroeder, 2013), when slow sensor

https://doi.org/10.5194/egusphere-2025-241
Preprint. Discussion started: 10 February 2025

response times meet temperature gradients during ascent (and descent). These errors can be corrected if the sensor's time constant is well known (Cassano, 2014), but this requires rigid filtering of high-frequency noise, which can also eliminate information about small-scale turbulence. A fast sensor is always preferable for accurate soundings. Unlike radiosonde sensors, our sensor is not exposed to very low temperatures and pressures, which are particularly unfavorable conditions. The SWUF-3D fleet is designed for boundary-layer operation in non-precipitation conditions and can therefore be optimized for these conditions. Figure 7 shows two examples of vertical profiles measured simultaneously with an HYT sensor and a FWPRT. The hysteresis caused by the HYT sensor's time response is clearly evident in Fig. 7a) and results in a temperature offset of almost 1°C between ascent and descent. No hysteresis is observed with the FWPRT sensor (red curves). The FWPRT data does indicate that more turbulent fluctuations are observed during ascent, likely due to mixing by rotor downwash during descent. The dotted blue lines show a time-lag-corrected version of the HYT measurements, which shows good agreement in this case with a constant temperature gradient. Figure 7b) provides an example of a more complex boundary layer in the early morning, where a nighttime inversion is still present but is being slowly eroded by surface heating below 100 m. During this flight, the vertical profile was interrupted at a height of 100 m for 10 s, which is clearly reflected in a temperature adjustment for the slow sensor (dark blue line) due to its response time. Time response correction brings the slow sensor's curves significantly closer to the fast sensor's curves but is highly sensitive to the applied time constant and can therefore introduce large errors. Both examples demonstrate the importance of fast temperature sensors for profiling the atmospheric boundary layer with the goal of resolving small-scale structures, accurate inversions, and temperature gradients.

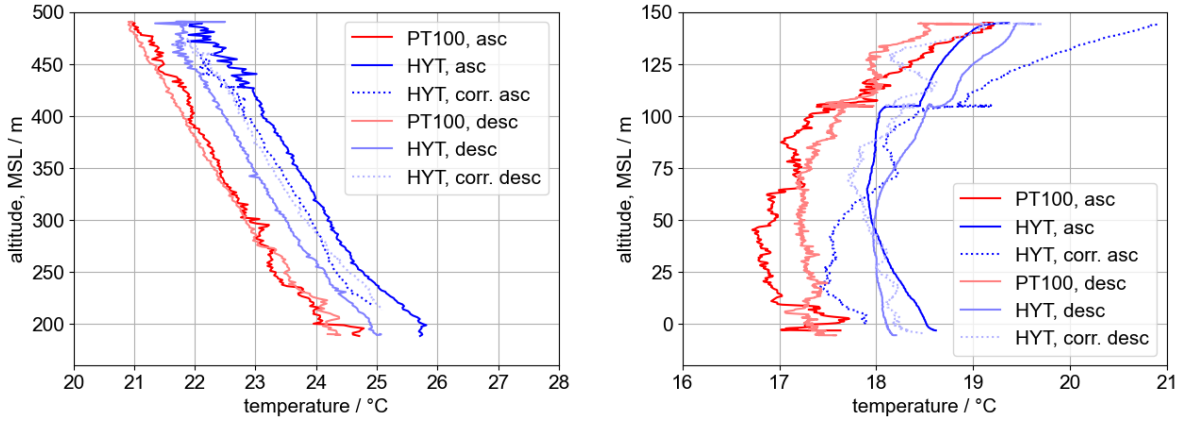

Figure 7. Vertical profile at Cochstedt airport. Comparison between SWUF-T fine-wire sensor (red) and HYT temperature sensor with (blue, dotted) and without (blue, solid) time constant correction. a) shows a vertical profile up to 300 m at the Cochstedt airport on 25 June 2024, 15:00 UTC, b) shows a vertical profile up to 150 m at Krummendeich in the early morning of 22 July 2024, 04:40 UTC.

https://doi.org/10.5194/egusphere-2025-241
Preprint. Discussion started: 10 February 2025

Table 3. Calibration flight results.

Flight #69						
Variable	Sonic	QAV32	QAV12	QAV13	QAV14	QAV15
$\overline{T}$ / °C	16.3	16.3	16.4	16.3	16.3	16.3
σ_T^2 / K^2	0.013	0.017	0.0028	0.021	0.03	0.019
σ_w^2 / m^{2}s^{-2}	0.3	0.47	0.1	0.43	0.49	0.62
H / W m^{-2}	35	59	NA	70	98	73
Flight #70						
Variable	Sonic	QAV21	QAV22	QAV23	QAV24	QAV25
$\overline{T}$ / °C	16.6	16.5	16.4	16.3	16.5	16.3
σ_T^2 / K^2	0.044	0.019	0.041	0.041	0.058	0.054
σ_w^2 / m^{2}s^{-2}	0.76	0.58	0.65	0.67	0.76	0.48
H / W m^{-2}	124	12	126	133	133	129

5.4 Turbulence measurements

We developed and integrated the SWUF-T module into the SWUF-3D fleet with the primary goal of resolving small-scale turbulent temperature fluctuations and determining second-order statistics with accuracy comparable to that of other in situ instrumentation. This chapter presents the results of in-flight tests of the SWUF-T module, comparing its measurements with those from sonic anemometers at the MMA in the WiValdi research park.

5.4.1 Inter-drone comparison

The calibration flight pattern with five drones spaced 8 m apart (see Sect. 5.2) is well suited for intercomparison of turbulence measurements from the ten drones used in the fleet. We calculate mean temperature ($\overline{T}$), temperature variance (σ_T^2), vertical wind speed variance (σ_w^2), and sensible heat flux (H) for the five drones during flights #69 and #70. QAV12 exhibited some temperature reading dropouts during these flights, which particularly affected the variance estimation; therefore, its data is grayed out. The temperature sensor of QAV21 consistently showed low variance values throughout the campaign, a problem identified through this test and is likely due to problems with the platinum wire. While QAV12 can still be used in flights without temperature sensor dropouts, QAV21 is excluded from further analysis in this study. The agreement of variance and sensible heat flux estimates from the drones in flight #70 is very good within the fleet and compared to the sonic anemometer ($\Delta H < 10$ W m^{-2}). During flight #69, lower turbulence was observed; consequently, the drones show an overestimation of variances and heat flux ($\overline{\Delta H} = 40$ W m^{-2}) for this flight. We attribute this to the physical limitations of turbulence measurement at small scales with these drones in their current state of development. Table 3 presents all derived values for the calibration flights.

Figure 8 shows the variance spectra for flight #70. The spectra of the four SWUF-T sensors (red) follow the Kolmogorov $-5/3$-slope and the sonic anemometer reference well up to the Nyquist frequency of 2 Hz, which is half the sampling frequency

https://doi.org/10.5194/egusphere-2025-241
Preprint. Discussion started: 10 February 2025

that was set to 4 Hz for the experiment. There is only a small underestimation over the whole frequency range in this case. We also show the slow HYT-sensor in comparison (green) which are unable to resolve turbulence scales appropriately above 10^{-2} Hz. This illustrates the huge improvement with the new sensors.

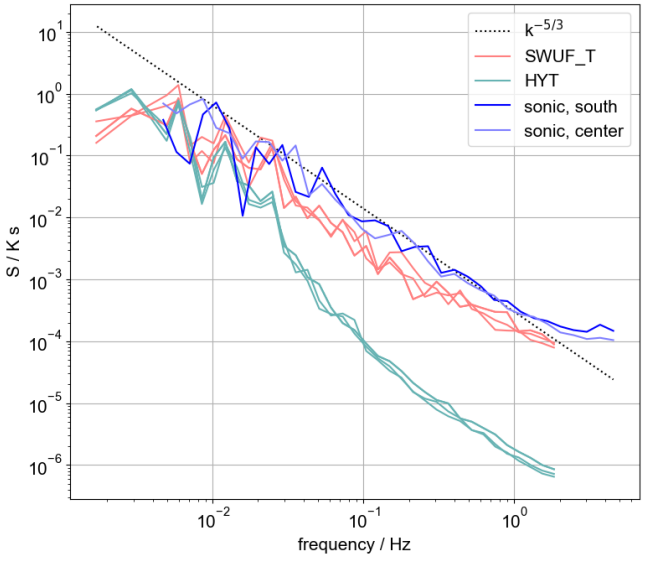

Figure 8. Spectra of virtual temperature for one UAS flight next to a sonic anemometer showing measurements of the sonic (gray), the slow HYT271 (blue) sensor and the FWPRT (red).

5.4.2 Comparison to MMA

For all flights listed in Table 1, we determined the temperature variance during the drone hover periods and the corresponding time periods of the sonic anemometers at the mast array.

Figure 9b shows a scatter plot of this comparison, separating measurements at 25 m (blue) and 99 m (red) above ground level. A correlation coefficient of $R^2 = 0.89$ is achieved. At higher variance values, the scatter increases slightly. This may be attributable to the increasing effect of spatial separation between the UAS and mast under conditions of higher turbulence. We also do not correct for the advective time delay between the sensors, which contributes to the error but is impossible to eliminate perfectly in a boundary layer with turbulence intensity exceeding 15%. To provide an indication of the achievable agreement under these conditions, we also present a comparison between the two sonic anemometers at the north and south masts of the MMA. The resulting correlation coefficient is slightly lower, at $R^2 = 0.83$. This demonstrates that the uncertainty of the experimental setup exceeds the uncertainty of the sensors themselves and therefore does not represent the actual limit of accuracy; however, it does show that the sensor uncertainty is equal to or smaller than the experimental uncertainty.

https://doi.org/10.5194/egusphere-2025-241
Preprint. Discussion started: 10 February 2025

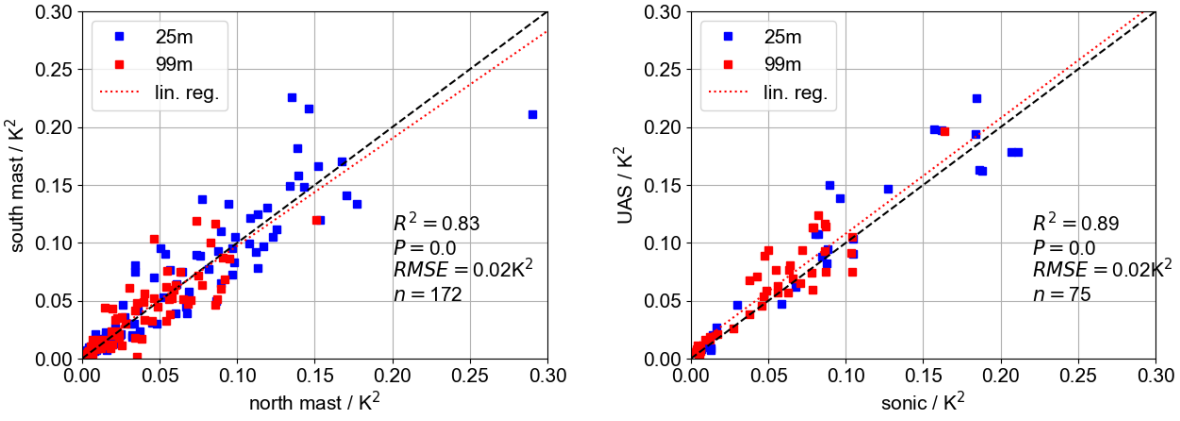

Figure 9. Comparison of temperature variance between sonic anemometers of north and south mast (a) and between UAS and the closest mast (b). Shown are the comparisons at 25 m level (blue) and 99 m level (red). The linear regression is shown as red dotted line.

5.4.3 Sensible heat flux

With fast temperature measurements and simultaneous vertical wind measurements, as demonstrated in Wildmann and Wetz (2022), sensible heat flux calculations are possible if the dominant scales for turbulent transport are large enough to be sampled at a 2 Hz temporal resolution (i.e., approximately 2…5 m eddy size at 4…10 m s^{-1}).

Several boundary conditions must be considered when comparing sensible heat flux measurements from the SWUF-3D UAS and sonic anemometers at the MMA:

1. Only conditions with horizontal wind speeds below 8 m s^{-1} should be considered because vertical wind speed measurements from the drones are unreliable at higher wind speeds with the current vertical wind estimation algorithm.
2. Sensible heat flux in the ABL can be highly variable in time and space, and the 10-minute flight periods do not necessarily represent stationary conditions but may include transient flows.
3. No study has yet examined the effect of the masts and guy wires on turbulence measurements at the MMA; therefore, the sonic anemometer reference may also contain errors. The UAS flights in this study were conducted with wind directions from 200–300°, minimizing the likelihood of major disturbances.

To establish a benchmark for the expected uncertainty in a comparative experiment, we present a comparison between two sonic anemometers at the MMA - specifically, one at 99 m on the south mast and one at 99 m on the north mast (see Fig. 10a). Although these two masts are only 100 m apart, the correlation coefficient between sensible heat flux estimates is only $R^2 \approx 0.64$. Figure 10b shows the comparison of each available UAS flight meeting the filter criteria with the closest sonic anemometer (typically at a distance of $d \approx 50$ m). The correlation is of a similar magnitude as that between the masts ($R^2 = 0.72$). The RMSE are 41 W m−2 and 47 W m−2 respectively. As with the variance comparison, this indicates that the

https://doi.org/10.5194/egusphere-2025-241
Preprint. Discussion started: 10 February 2025

accuracy of the drone measurements falls within the uncertainty of the experimental setup. Figure 10b shows the scatter plot of the UAS measurements compared with the sonic anemometer measurements. As in the calibration flight example, very low heat fluxes are overestimated by the drones, and scatter increases with higher H values. The outliers at 25 m can be attributed to measurements with QAV15 on 22 July and will be discussed below. In the figure, all calculated values are shown in light colors, while dark/full colors represent only those values remaining after filtering for wind speeds exceeding 8 m s^{-1}. This shows that vertical wind speed variance is a significant source of uncertainty for flux measurements with the SWUF-3D fleet.

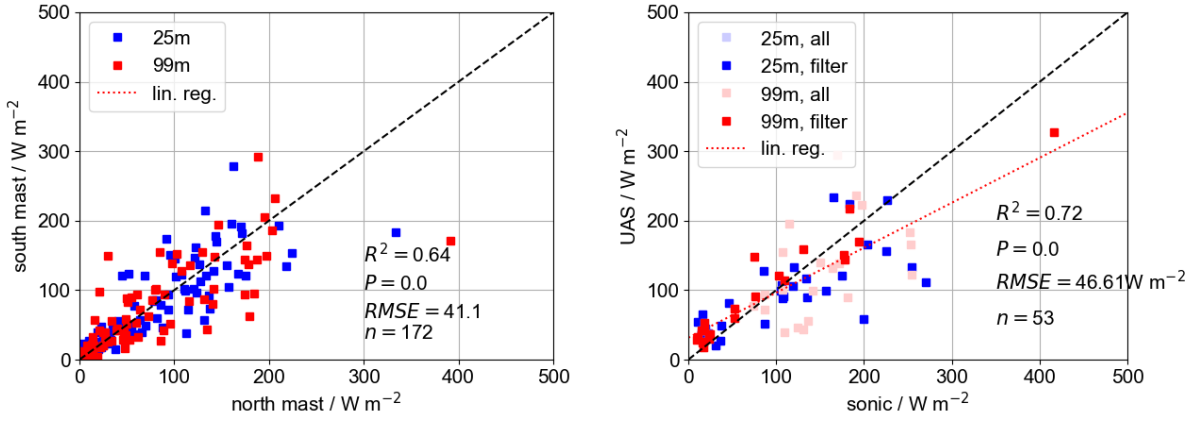

Figure 10. Comparison of sensible heat flux between sonic anemometers of north and south mast (a) and between UAS and the closest mast (b). Shown are the comparisons at 25 m level (blue) and 99 m level (red). The linear regression is shown as red dotted line.

Figure 11 shows the time series of measured and derived variables for 22 July 2024, the day with the most consecutive flights between 10:00 UTC and 16:00 UTC. On the left, drones at 25 m hover height are compared to the corresponding sonic anemometers at the same height. For this height and day, mainly two drones, i.e. QAV15 (light red circles) and QAV25 (dark red stars), were measuring without technical problems of the temperature sensors, while QAV21 and QAV32 at the northern mast did have failures. QAV15 is placed west of the mast and QAV25 on the east. The plot reveals several interesting observations:

- The SWUF-T sensors accurately capture the long-term temperature trend.
- The temporal variation of temperature variance at 25 m is substantial, meaning that small offsets in time and space can lead to significant errors in direct comparisons between sonic anemometer and drone measurements. The same applies to vertical wind speed variance at 99 m.
- QAV15 exhibits an underestimation of heat flux, possibly indicating a local effect, because it cannot be observed on other days and for other drones. It is notable that for the early flights, wind direction is almost perfectly in line with drones and mast. The surface below drone QAV15 is corn at low height, while the mast and drone QAV25 are above the dirt road. At such low heights this might have an effect on the measured heat fluxes.

https://doi.org/10.5194/egusphere-2025-241
Preprint. Discussion started: 10 February 2025

– The drones slightly overestimate vertical wind speed variance at 99 m, likely due to the stronger wind speeds at that height. The data in this plot has not been filtered for high wind speeds.

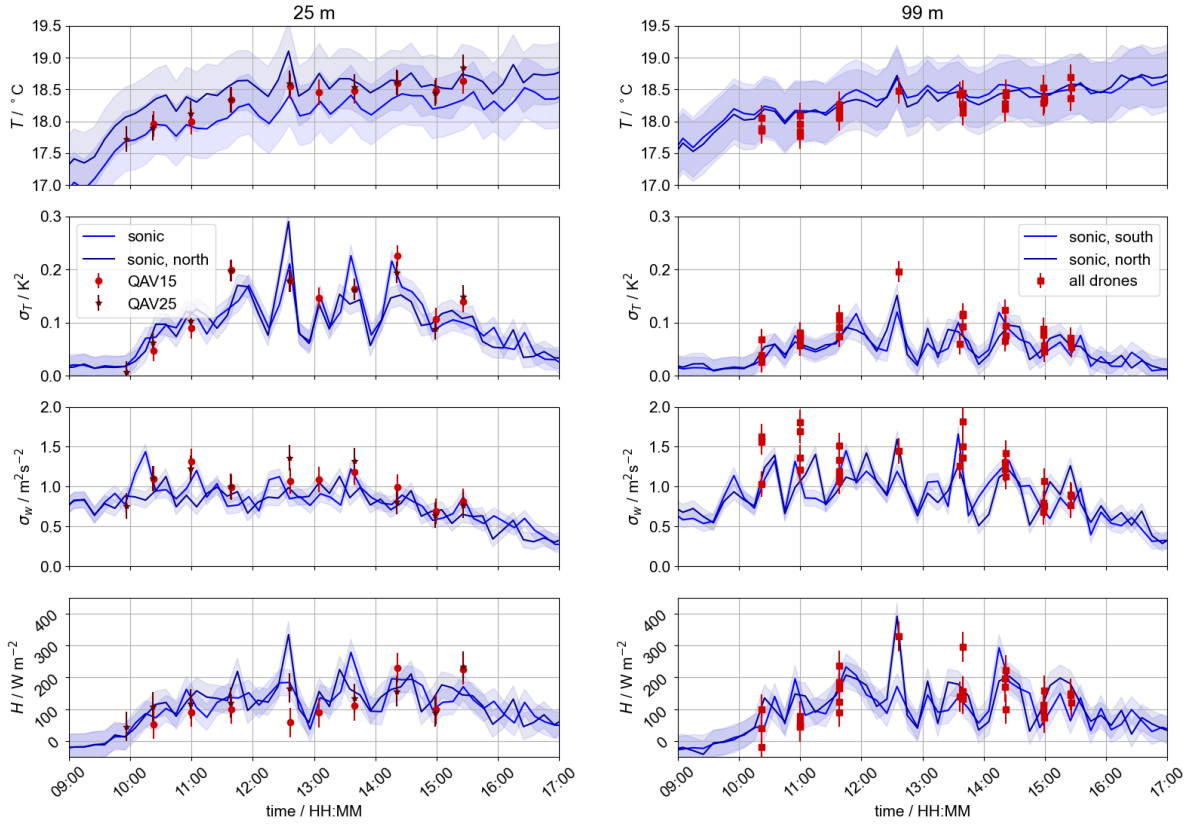

Figure 11. Time series of temperature T (a,e), temperature variance σ_T^2 (b,f), vertical wind speed variance σ_w^2 (c,g) and sensible heat flux H (d,h) for 22 July 2024. 10-minute averaged sonic anemometer measurements on south (dark blue) and north mast (light blue) are compared to drone measurements (red squares).

6 Conclusions

This study has demonstrated the feasibility of robust temperature measurements using self-calibrated fine-wire resistance thermometers (FWPRTs) integrated into the SWUF-3D UAS fleet. Key findings and conclusions are summarized below:

Turbulent temperature fluctuations at scales larger than 1 m can be effectively measured using the SWUF-3D fleet equipped with SWUF-T sensor modules. The physical limits are probably not even reached, since platinum wires with the used diameter have been shown to resolve scales up to 10 Hz (Wildmann et al., 2013), but sampling rate was limited to 5 Hz for the SWUF-T sensors at this point. We conclude that rotor-induced flow disturbance does not appear to significantly impact temperature

https://doi.org/10.5194/egusphere-2025-241
Preprint. Discussion started: 10 February 2025

measurements, even with the sensor positioned close to the rotor plane, provided it remains aligned with the wind direction. Compared to slower solid-state sensors, the SWUF-T FWPRT represent a substantial improvement for vertical temperature gradient profiling in the ABL. The absence of hysteresis between ascent and descent allows both flight phases to be used for future investigations of boundary-layer development.

While calculating turbulent fluxes using the eddy covariance method is possible, it is susceptible to errors in both temperature and vertical wind speed measurements. The experimental setup, characterized by high wind speeds and turbulence intensity, presented challenges in precisely quantifying the uncertainty of flux measurements with the SWUF-3D fleet. The spatial variability of sensible heat flux, calculated from 10-minute averages, was found to be on the order of 41 W m^{-2}, comparable to the observed RMSE for the drone measurements (47 W m^{-2}).

Future work should focus on extending flight times (beyond 30 minutes) and conducting measurements under more stationary flow conditions and a wider range of atmospheric conditions to enhance confidence in the results and refine uncertainty estimates. The analysis revealed that uncertainties in sensible heat flux are to a large degree related to uncertainties in vertical wind speed estimation, particularly at high wind speeds, where vertical flux estimates cannot currently be considered reliable. Further improvements to vertical wind speed measurement are therefore crucial for reducing flux measurement uncertainty.

Comparisons with the meteorological mast array (MMA) proved challenging due to uncertainties in the sonic anemometers' temperature and wind measurements under varying inflow conditions. Further investigation of flow around the MMA should be performed, for which the SWUF-3D fleet itself presents a valuable tool.

Despite these challenges, the flexibility and robustness of the SWUF-3D fleet are significant assets. Its deployment in future field campaigns, particularly in locations where traditional mast-based instrumentation is infeasible, will be of great importance. Finally, quantifying the uncertainty of individual UAS measurements will facilitate the propagation of these uncertainties to spatial correlation and flux measurements, a capability offered by the SWUF-3D fleet.

Data availability. Data of the MMA and IEC mast are stored in the archive of the WiValdi wind park. Drone data will in future be stored in these archives as well, but may be made available by the authors upon request.

Author contributions. NW designed and built the first SWUF-T sensors, did the data analyses and writing of the paper. LG contributed to the calibration of the sensors and the corresponding section in the manuscript.

Competing interests. We declare no competing interests.

https://doi.org/10.5194/egusphere-2025-241
Preprint. Discussion started: 10 February 2025

Acknowledgements. This research has been supported by the HORIZON EUROPE European Research Council (grant no. 101040823, ESTABLIS-UAS). This work was partly accomplished within the research project Deutsche Forschungsplattform für Windenergie (http://dfwind.de). We greatly acknowledge the financial support of the German Federal Ministry for Economic Affairs and Climate Action, through FKZ 0325936, that enabled this work. We acknowledge the support by the DLR-WX and DLR-UX teams in supporting the campaigns. We especially thank Johannes Kistner and Almut Alexa for their hard work in preparing and carrying out the campaigns at Krummendeich and Cochstedt. We thank Paula Hofmann, Paul Waldmann, Michael Lichtenstern and Anke Roiger for the support with smoke plume visualization and providing the video of this test. The authors acknowledge the use of a large language model (e.g., Gemini and llama3.2) for language improvements.

https://doi.org/10.5194/egusphere-2025-241
Preprint. Discussion started: 10 February 2025

References

Boventer, J., Bramati, M., Savvakis, V., Beyrich, F., Kayser, M., Platis, A., and Bange, J.: Validation of Doppler Wind Lidar Measurements with an Uncrewed Aircraft System (UAS) in the Daytime Atmospheric Boundary Layer, Journal of Atmospheric and Oceanic Technology, 41, 705 – 723, https://doi.org/10.1175/JTECH-D-23-0127.1, 2024.

Cassano, J. J.: Observations of atmospheric boundary layer temperature profiles with a small unmanned aerial vehicle, Antarctic Science, 26, 205–213, https://doi.org/10.1017/S0954102013000539, 2014.

de Boer, G., Borenstein, S., Calmer, R., Cox, C., Rhodes, M., Choate, C., Hamilton, J., Osborn, J., Lawrence, D., Argrow, B., and Intrieri, J.: Measurements from the University of Colorado RAAVEN Uncrewed Aircraft System during ATOMIC, Earth System Science Data, 14, 19–31, https://doi.org/10.5194/essd-14-19-2022, 2022.

Ghirardelli, M., Kral, S. T., Müller, N. C., Hann, R., Cheynet, E., and Reuder, J.: Flow Structure around a Multicopter Drone: A Computational Fluid Dynamics Analysis for Sensor Placement Considerations, Drones, 7, https://doi.org/10.3390/drones7070467, 2023.

Hervo, M., Romanens, G., Martucci, G., Weusthoff, T., and Haefele, A.: Evaluation of an Automatic Meteorological Drone Based on a 6-Month Measurement Campaign, Atmosphere, 14, https://doi.org/10.3390/atmos14091382, 2023.

Jin, L., Ghirardelli, M., Mann, J., Sjöholm, M., Kral, S. T., and Reuder, J.: Rotary-wing drone-induced flow – comparison of simulations with lidar measurements, EGUsphere, 2023, 1–21, https://doi.org/10.5194/egusphere-2023-1546, 2023.

Kistner, J., Neuhaus, L., and Wildmann, N.: High-resolution wind speed measurements with quadcopter uncrewed aerial systems: calibration and verification in a wind tunnel with an active grid, Atmospheric Measurement Techniques, 17, 4941–4955, https://doi.org/10.5194/amt-17-4941-2024, 2024.

Lappin, F., de Boer, G., Klein, P., Hamilton, J., Spencer, M., Calmer, R., Segales, A. R., Rhodes, M., Bell, T. M., Buchli, J., Britt, K., Asher, E., Medina, I., Butterworth, B., Otterstatter, L., Ritsch, M., Puxley, B., Miller, A., Jordan, A., Gomez-Faulk, C., Smith, E., Borenstein, S., Thornberry, T., Argrow, B., and Pillar-Little, E.: Data collected using small uncrewed aircraft system during the TRacking Aerosol Convection Interactions ExpeRiment (TRACER), Earth System Science Data Discussions, 2023, 1–23, https://doi.org/10.5194/essd-2023-371, 2023.

Lappin, F. M., Bell, T. M., Pillar-Little, E. A., and Chilson, P. B.: Low-level buoyancy as a tool to understand boundary layer transitions, Atmospheric Measurement Techniques, 15, 1185–1200, https://doi.org/10.5194/amt-15-1185-2022, 2022.

Lee, T. R., Buban, M., Dumas, E., and Baker, C. B.: A New Technique to Estimate Sensible Heat Fluxes around Micrometeorological Towers Using Small Unmanned Aircraft Systems, Journal of Atmospheric and Oceanic Technology, 34, 2103 – 2112, https://doi.org/10.1175/JTECH-D-17-0065.1, 2017.

Lenschow, D., Society, A. M., and for Atmospheric Research (U.S.), N. C.: Probing the atmospheric boundary layer, American Meteorological Society, ISBN 9780933876637, 1986.

Liu, H., Peters, G., and Foken, T.: New Equations For Sonic Temperature Variance And Buoyancy Heat Flux With An Omnidirectional Sonic Anemometer, Boundary-Layer Meteorology, 100, 459–468, https://doi.org/10.1023/A:1019207031397, 2001.

Pfister, L., Gohm, A., Kossmann, M., Wieser, A., Babić, N., Handwerker, J., Wildmann, N., Vogelmann, H., Baumann-Stanzer, K., Alexa, A., Lapo, K., Paunović, I., Leinweber, R., Sedlmeier, K., Lehner, M., Hieden, A., Speidel, J., Federer, M., and Rotach, M.: The TEAMx?PC22 Alpine field campaign ? Objectives, instrumentation, and observed phenomena, Meteorologische Zeitschrift, 33, 199–228, https://doi.org/10.1127/metz/2024/1214, 2024.

https://doi.org/10.5194/egusphere-2025-241
Preprint. Discussion started: 10 February 2025

Segales, A. R., Greene, B. R., Bell, T. M., Doyle, W., Martin, J. J., Pillar-Little, E. A., and Chilson, P. B.: The CopterSonde: an insight into the development of a smart unmanned aircraft system for atmospheric boundary layer research, Atmospheric Measurement Techniques, 13, 2833–2848, https://doi.org/10.5194/amt-13-2833-2020, 2020.

Segales, A. R., Chilson, P. B., and Salazar-Cerreño, J. L.: Considerations for improving data quality of thermo-hygrometer sensors on board unmanned aerial systems for planetary boundary layer research, Atmospheric Measurement Techniques, 15, 2607–2621, https://doi.org/10.5194/amt-15-2607-2022, 2022.

Tikhomirov, A. B., Lesins, G., and Drummond, J. R.: Drone measurements of surface-based winter temperature inversions in the High Arctic at Eureka, Atmospheric Measurement Techniques, 14, 7123–7145, https://doi.org/10.5194/amt-14-7123-2021, 2021.

Tschudin, M. E. and Schroeder, S. R.: Time Constant Estimates for Radiosonde Temperature Sensors, Journal of Atmospheric and Oceanic Technology, 30, 40 – 56, https://doi.org/10.1175/JTECH-D-11-00181.1, 2013.

van den Kroonenberg, A. C., Martin, T., Buschmann, M., Bange, J., and Vörsmann, P.: Measuring the Wind Vector Using the Autonomous Mini Aerial Vehicle M^2AV, Journal of Atmospheric and Oceanic Technology, 25, 1969–1982, 2008.

Wetz, T. and Wildmann, N.: Spatially distributed and simultaneous wind measurements with a fleet of small quadrotor UAS, Journal of Physics: Conference Series, 2265, 022 086, https://doi.org/10.1088/1742-6596/2265/2/022086, 2022.

Wildmann, N. and Wetz, T.: Towards vertical wind and turbulent flux estimation with multicopter UAS, EGUsphere, 2022, 1–20, https://doi.org/10.5194/egusphere-2022-110, 2022.

Wildmann, N., Mauz, M., and Bange, J.: Two fast temperature sensors for probing of the atmospheric boundary layer using small remotely piloted aircraft (RPA), Atmospheric Measurement Techniques, 6, 2101–2113, https://doi.org/10.5194/amt-6-2101-2013, 2013.

Wildmann, N., Rau, G. A., and Bange, J.: Observations of the Early Morning Boundary-Layer Transition with Small Remotely-Piloted Aircraft, Boundary-Layer Meteorology, 157, 345–373, https://doi.org/10.1007/s10546-015-0059-z, 2015.